J Mol Model (2006) 12: 835–845
DOI 10.1007/s00894-006-0110-6

ORIGINAL PAPER

Raimundo Gargallo · Juan Cedano · Angel Mozo-Villarias · Enrique Querol · Baldomero Oliva

Study of the influence of temperature on the dynamics of the catalytic cleft in 1,3-1,4-β-glucanase by molecular dynamics simulations

Received: 23 June 2005 / Accepted: 10 January 2006 / Published online: 9 March 2006

Abstract The dependence of some molecular motions in the enzyme 1,3-1,4-β-glucanase from *Bacillus licheniformis* on temperature changes and the role of the calcium ion in them were explored. For this purpose, two molecular dynamics simulated trajectories along 4 ns at low (300 K) and high (325 K) temperatures were generated by the GROMOS96 package. Several structural and thermodynamic parameters were calculated, including entropy values, solvation energies, and essential dynamics (ED). In addition, thermoinactivation experiments to study the influence of the calcium ion and some residues on the activity were conducted. The results showed the release of the calcium ion, which, in turn, significantly affected the movements of loops 1, 2, and 3, as shown by essential dynamics. These movements differ at low and high temperatures and affect dramatically the activity of the enzyme, as observed by thermoinactivation studies.

The first two authors contributed equally to this work

R. Gargallo
Department of Analytical Chemistry, Universitat de Barcelona, Martí i Franquès 1-11, Barcelona 08028, Spain

J. Cedano · E. Querol
Institut de Biotecnologia i Biomedicina and Departament de Bioquímica i Biología Molecular, Universitat Autònoma de Barcelona, Bellaterra, Barcelona 08193, Spain

A. Mozo-Villarias
Departament de Ciències Mèdiques Bàsiques, Facultat de Medicina, Universitat de Lleida, Lleida 25198, Spain

B. Oliva (✉)
Grup de Bioinformàtica Estructural (GRIB-IMIM). Departament de Ciències Experimentals i de la Salut, Universitat Pompeu Fabra, Dr. Aiguader, 80, 08003 Barcelona, Catalonia, Spain
e-mail: boliva@imim.es
Fax: +34-932240875

Keywords Enzyme deactivation · Reaction field · Essential dynamics · Thermoinactivation · Structural alignment

Abbreviations MD: Molecular dynamics · RF: Reaction field · RMSD: Root mean square deviation · ED: Essential dynamics

Introduction

Endo-1,3-1,4-β-glucanase from *Bacillus licheniformis* is a 24 kDa enzyme that catalyzes the hydrolysis of β-glucans containing mixed β-1,3 and β-1,4 linkages such as lichenan and barley β-glucan. This enzyme is classified as one of the family of 16 glycosyl hydrolases, and has a topology consisting mainly of two eight-stranded antiparallel β-sheets arranged in a jellyroll β-sandwich (Fig. 1). The catalytic residues are located on the concave side of the protein and have been characterized by site-directed mutagenesis [1, 2]. The hydrolytic mechanism of the glycosidic bond of this enzyme is based on a general acid/base catalysis with a net retention of the anomeric configuration [3, 4]. Experiments indicated that Glu105 acts as a nucleophile (which binds covalently to the substrate), while Glu109 is the general-acid catalyst, and that Asp107 is also crucial for activity (it may affect the acid properties of Glu109 strongly) [2, 5].

A calcium ion is located at the opposite side of the catalytic cleft, on the convex side of the protein. The crystal of *B. licheniformis* 1,3-1,4-β-glucanase shows calcium exhibiting octahedral coordination geometry to the backbone carbonyl oxygens of Pro9, Gly45, and Asn207, an amide oxygen of Asn207. This calcium ion plays an important role in stabilizing the native protein structure [6, 7]. The half transition temperatures are higher in the presence of Ca^{2+} than in Ca^{2+}-free buffer [8]. Removal of the bound calcium had a dramatic effect on thermal stability, and replacement of Ca^{2+} by Na^{+} notably reduced the half-life of the protein [9]. The influence of calcium on thermal stability was analyzed by microcalorimetric

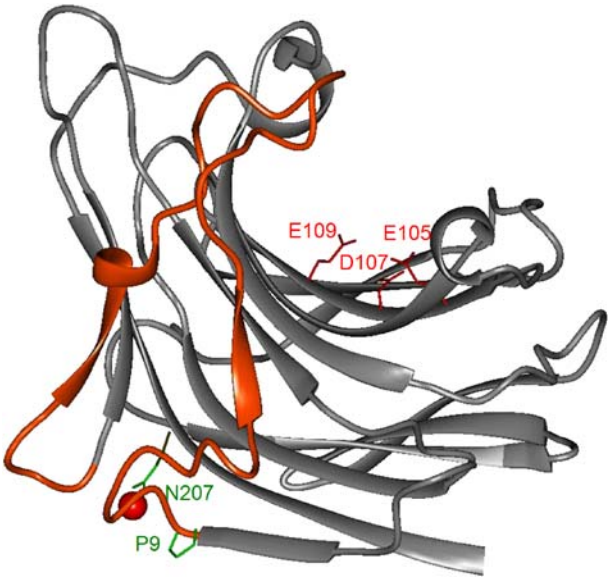

Fig. 1 Crystallographic structure of 1-3;1-4 β-glucanase from *Bacillus licheniformis* at 1.8 Å resolution (PDB code 1GBG). The catalytic residues (E105, D107, and E109) located on the concave side are colored in *red*. Loop 1 is drawn in *orange*. Residues P9, G45, and N207, and calcium ion are colored in *green* and *red*, respectively

measurements in wild type, *B. amyloliquefaciens*, and *B. macerans* as well as in several hybrids. Hybrids consist mainly of the amino-acid sequence of *B. macerans* and short N-terminal segments from 12 to 16 amino-acid residues length derived from *B. amyloliquefaciens*. The exchange of a few amino-acid residues near the N-terminus of the *B. macerans* glucanase, where the Ca^{2+} binding site is located, seems to influence the thermal stability of the hybrids very strongly [7]. *Bacillus* 1,3-1,4-β-glucanases usually possesses a single disulphide bridge that connects a β-strand of the concave side of the β-sandwich with a long loop. Finally, *B. licheniformis* 1,3-1,4-β-glucanase can be considered a thermostable protein, active at room temperature, inactive at 65°C, and with the optimum temperature for enzyme activity around 55°C [10].

We explored the possibility of examining the thermal inactivation process of the β-glucanase using molecular dynamics (MD) simulations. This type of approach is especially interesting when the process of inactivation of an enzyme has an active intermediate because in this case, we can identify an intermediate stable state of the protein different from the native protein conformation. The behavior of the calcium ion and its role in the activity of the enzyme were studied. Essential dynamics (ED), a useful tool for the study of dynamics in proteins [11–13], was also used to study how the motions of the protein change as temperature rises.

Materials and methods

Parameters for molecular dynamics simulations

The crystallographic coordinates of 1-3;1-4 β-glucanase from *B. licheniformis* at 1.8 Å resolution (PDB code 1GBG) were used to seed the simulations. The active site was found in residues E105, D107, E109, the main regions—loop 1, defined as the fragment between residues 9 and 45 and loop 3, defined as the fragment between 185 and 210, both at the top of the active site—and the intermediate fragment, loop 2, between residues 51–60 and positioned between loops 1 and 3. A total of nine Na^+ and 11 Cl^- ions were added to neutralize some of the charges of Asp/Glu and Arg/Lys residues. The crystallographic Ca^{2+} ion formed a cluster with residues P9, G45, and N207 found between the β-strands 1, 4, and 15, respectively. The total amount of ions was chosen to keep the complete system neutralized. The total number of protein atoms was 2,270, the number of ions 21, the amount for positive charges nine Na^+ ions, and the amount for negative charges 11 Cl^- ions. After 1 ns of simulation, the system became equilibrated, but several Cl^- ions were found in the surroundings of the Ca^{2+} ion. This situation produced a metastable equilibrium easily perturbed by increasing the temperature. Therefore, the total ionic strength was reduced and seven Na^+ and eight Cl^- were removed to maintain the electrostatic equilibrium stabilized at a lower ionic strength. Several simulations were performed to test the consistency of the final ionic strength by relocating the ions without this stabilization. However, with the exception of the seeding-optimized model formed by the solvated protein plus ions, all of them yielded the loss of the Ca^{+2} ion at standard temperature.

The solute system was embedded in a box of 62×65×74 $Å^3$ with 8,750 water molecules and periodic boundary conditions were applied. The GROMOS96 program [14] was used to perform the explicit solvent simulations using the GROMOS 43a1 force field and the SPC/E water model [15].

To compare the active and inactive states of the enzyme, two MD-simulations were carried out under a Berendsen's coupling bath at 300 and 325 K. We used a separate coupling for water molecules and solute molecules (enzyme plus counterions) with a 0.1-ps relaxation time. We also allowed for kinetic fluctuations that implied about 10°C increase in the temperature. Therefore, due to the fluctuation of the solute kinetic energy along the simulation, the inner temperature of the enzyme was allowed to reach values around 37 or 62°C in each simulation at 300 and 325 K, respectively. This would represent the experimental conditions at which the enzyme is active and inactive, respectively.

A seeding simulation was run for 1,000 ps using a time step of 0.002 ps at 1 atm and 300 K with Berendsen's coupling bath (relaxation times of 0.1 ps for temperature and 0.5 ps for pressure) to maintain isothermic-isobaric conditions. At 1,000 ps, a second simulation was started by continuing the seeding simulation on a bath at 325 K. Both simulations, at 300 and 325 K, did continue for 3,000 ps more. Bond lengths were constrained by SHAKE [16] and nonbonded interactions were calculated with the twin-range method. All interactions were calculated under a cutoff of 9 Å and a list of atoms (updated every 0.02 ps) was used to calculate long range interactions between 9 and 12 Å. An

additional term for long range electrostatic interactions was applied according to the reaction field (RF) procedure. In the RF approach, the electrostatic interaction energy between two charges q_i and q_j is obtained by Coulomb plus monopolar and dipolar terms of a reaction field. The additional terms are dependent on: (1) a radius for the field (R_{rf}) and (2) a coefficient determining the magnitude of the reaction field forces that is defined by the surrounding environment (C_{rf}) [17–19]. The radius of the field is set equal to R_l, being R_l the long-range cutoff distance, while the coefficient C_{rf} depends on the permittivity of the dielectric in vacuum (ε_1=1) and the relative dielectric permittivity of the dielectric continuum (ε_2=54 as appropriate for the solvent model used in the simulations).

The MD simulations were carried out using a parallel version of GROMOS96 on an SGI Origin 2000 (CESCA-CEPBA, Barcelona, Spain) with 64 MIPS R10000 processors (each with 4 Mb cache) and 8 Gb of main memory.

Analysis of results from molecular dynamics simulations

Several structural properties of the system were analyzed as a function of time: the root-mean-square deviation from the original optimized structure (RMSD), the hydrogen-bond network within the protein, and the (polar and nonpolar) solvent-accessible surface area (SASA). The SASA was calculated according to a method described previously [20]. In addition, the atom-position deviation from the crystal structure was calculated.

Several thermodynamic quantities were also analyzed as a function of time: total potential energy, electrostatic energy, and estimates of solvation free energy and entropy of the protein. Solvation free energy was calculated using a finite-difference Poisson–Boltzmann algorithm [21], as implemented in macroscopic electrostatics with atomic detail (MEAD) [22].

The covariance matrix was calculated for the equilibrated portion of each trajectory (interval 2,000–4,000 ps) as the $3N\times3N$ matrix with elements

$$C = \sum_{k=1}^{M} \left\langle \left(x_i(k) - \langle x_i \rangle\right)\left(x_j(k) - \langle x_j \rangle\right) \right\rangle \quad (1)$$

where $x_i(k)$ is the atomic Cartesian coordinate of atom i in configuration k, after applying a least-squares-fit to a common reference structure (X-ray), and <xi> is the mean value of coordinates of atom i. An upper-bound estimate of the solute entropy was calculated according to the method proposed by Schlitter [23–26], as:

$$S = \frac{1}{2} k_B \mathrm{In}\ \det\left[1 + \frac{4\pi^2 \mathrm{k_B Te^2}}{\mathrm{h^2}} \mathrm{MC}\right] \quad (2)$$

where k_B is Boltzmann's constant, h Planck's constant, T the temperature, M is the diagonal $3N\times3N$ mass matrix, and C the covariance matrix of atom position fluctuations.

ED calculations were also based on the covariance matrix $\mathbf{C}$[10]. In this approach, the diagonalization of $\mathbf{C}$ to solve the equation

$$\Lambda = V^T C V \quad (3)$$

where $\mathbf{\Lambda}$ is a diagonal matrix, provides a set of $3N$ orthonormal Eigenvectors, $\mathbf{v}_n$ (the columns of the matrix $\mathbf{V}$) with their corresponding Eigenvalues λ_n (the diagonal elements of $\mathbf{\Lambda}$). The Eigenvectors represent the specific modes of structural deformation of the protein, while the Eigenvalue associated with a mode indicates the relative contribution of this mode to overall protein motion within the simulated trajectory.

Deformations associated with each Eigenvector were obtained by short MD trajectories along the major Eigenvectors generated according to the procedure described by Sherer et al. [27]. The trajectories were analyzed to identify the main contributions of each residue to each essential mode.

Experimental part

Bacterial strains E. coli TG1 (supE hsdΔ5 thi Δ(lac-proAB) F'[traD36 proAB+ lacIq lacZΔM15]) was used for pasmid propagation, transformation, and protein expression.

Oligonucleotides Mutants N207D and N207A were constructed by PCR-based site-directed mutagenesis (QuikChange site-directed mutagenesis kit, Stratagene) using these oligonucleotides: N207A (5′TTTACGCTCATTAtgcaTGG GTGCGTTACA3′ and 5′TGTAACGCACCCATGCATAA TGAGCGTAAA3′), N207D (5′TACGCTCATTACgAc TGGGTcCGTTACACAAAAA3′ and 5′TTTTTGTGTAA CGGACCCAGTCGTAATGAGCGTA3′).

Purification Mutants and wild-type were purified by experimental procedures described elsewhere [28].

Fluorescence measurements Transition temperatures (T_m) upon heating were measured spectrofluorimetrically on β-glucanase wild-type and N207D mutant in buffer 2 mM sodium cacodylate pH 6.0. Experiments were carried out with a Shimadzu RF2000 spectrofluorimeter.

Incubation The thermoinactivation method consists of deactivation of the protein contained in 75 μl enzyme solution (50 μg ml^{-1}), sodium acetate 50 mM, $CaCl_2$ 20 mM, and pH 6.0 in a 500 μl "eppendorf", by its incubation in a 65°C water bath. This temperature value was chosen because it produces a slow enzyme inactivation process [10].

Activity assays Enzyme activity was measured by the release of 4-methylumbelliferone at 365 nm with 3 mM of 4-methylumbelliferyl 3-*O*-β-cellobiosyl-β-D-glucopyranoside as substrate at 45°C in citrate–phosphate buffer (6.5 mM citric acid, 87 mM Na_2HPO_4) pH 7.2 and 0.1 mM $CaCl_2$ [29].

Results

Conformational analysis

Figure 2 shows the time series of the RMSD of the main-chain atoms. It shows that the conformation of glucanase varies with respect to the crystallographic structure more in the simulation at 325 than at 300 K, although without unfolding (RMSD lower than 2.5 Å). The RMSD shown in Fig. 2 indicates that the structure suffers a deviation of about 1 Å as soon as the temperature increases.

The surface accessibility for polar and nonpolar atoms was also calculated. The mean values of polar and nonpolar SASAs for both simulations are shown in Table 1. The comparison of the calculated values confirms that the conformation of glucanase did not unfold and the main solvation properties remained steady.

We checked the location of the calcium ion manually through the first 500 ps of the simulation at warm temperature. It showed similar binding to the simulation at 300 K. However, after 1 ns of simulation, loop-1 (between residues 9 and 45) deviated from the original conformation and increased the RMSD up to 2.5 Å in the following 2 ns. This deviation correlated with the release of the calcium ion from the protein, being embedded by the solvent. The situation for the calcium ion and loop-1 on the simulation at 300 K throughout this time (between 2 and 4 ns of the simulation) is steady, showing loop deviations of about 1 Å from the optimum seeding structure. The calcium cannot be bound again to its native location, and 4 ns simulation is sufficient to demonstrate the effect produced on the dynamic behavior of the protein after ion release. Also, we cannot insist on a possible protein unfolding, as this would take an extremely large simulation at this temperature (325 K) unless the temperature was increased to higher orders of magnitude (more than 400 K). Therefore, we could only record the details of the release of calcium caused by a small perturbation in the temperature of the system (25 K increase).

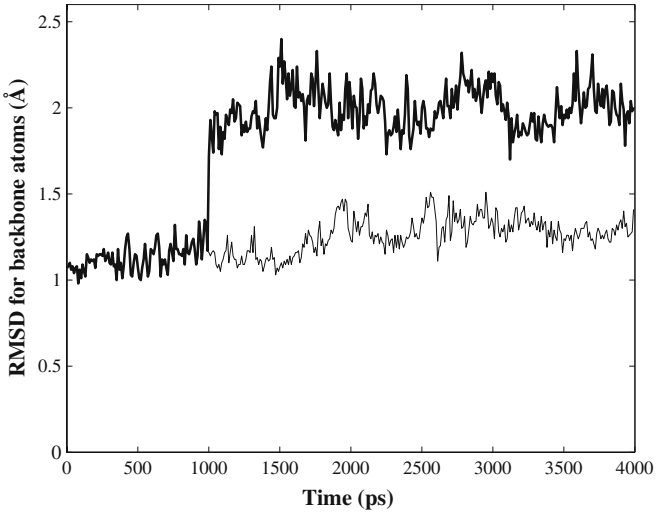

Fig. 2 RMSD time series. Time evolution of the root-mean-square atomic positional deviation (RMSD) from the crystallographic structure for backbone atoms. *Thin line*: low temperature simulation. *Thick line*: warm temperature simulation

Table 1 Solvent-accessible surface area (SASA)

Parameter		Simulation at 300 K	Simulation at 325 K
Total surface	($Å^2$)	10,203	10,163
Polar surface	($Å^2$)	6,408	6,334
	(%)	62.8	62.3
Non-polar surface	($Å^2$)	3,795	3,829
	(%)	37.2	37.7

Polar (O and N atoms), non-polar (C atoms), and total (polar plus non-polar) accessible area calculated as the sum of area for the corresponding atoms and its percentage. Averaged values during the 300 or 325 K simulation

Figure 3a shows temperature *B*-factors for the side chains as a function of residue number. The results were obtained from an average structure of the last 2,000 ps of every simulation. The *B*-factor values are quite similar for both simulations and the highest values are located at residues N26-N31 (extreme of loop 1), S53-K58 (extreme of loop 2), T95-P102 (near the 3_{10} helix, opposite loop 1), and N185-P201 (loop 3). Moreover, the Ca^{2+} ion shows a high *B*-factor value at warm temperature, which is related to the release of the ion from the protein. It should be stressed that the increase in temperature causes an increase in *B*-factor values for loop 1, and a decrease of *B*-factor values for loop 2, active site, and loop 3.

Hydrogen-bond network on the active loop

Table 2 shows the percentage of hydrogen bonds for loops 1 and 3, and in the β-strand of the active site. Overall, during the last 2 ns of the simulation at 300 K, the amount of hydrogen bonds retained is similar to that in the warm temperature simulation. However, about 10% of the hydrogen bonds involved in loops 1 and 3 and at the active site were lost for the simulation at warm temperature, mainly affecting the acceptor atoms on the backbone. The relation indicates that some changes occur on the surroundings of the active site.

To check the inner conformation of loop 1 between residues 9 and 45, involved with both calcium binding and active site top, the hydrogen bonding net was thoroughly analyzed. The result showed that most of the main-chain conformation was steady and the largest percentages of hydrogen bonds remained large at warm temperature, too. However, the analysis of the hydrogen bonds with low percentages at warm temperature showed that the β-strand

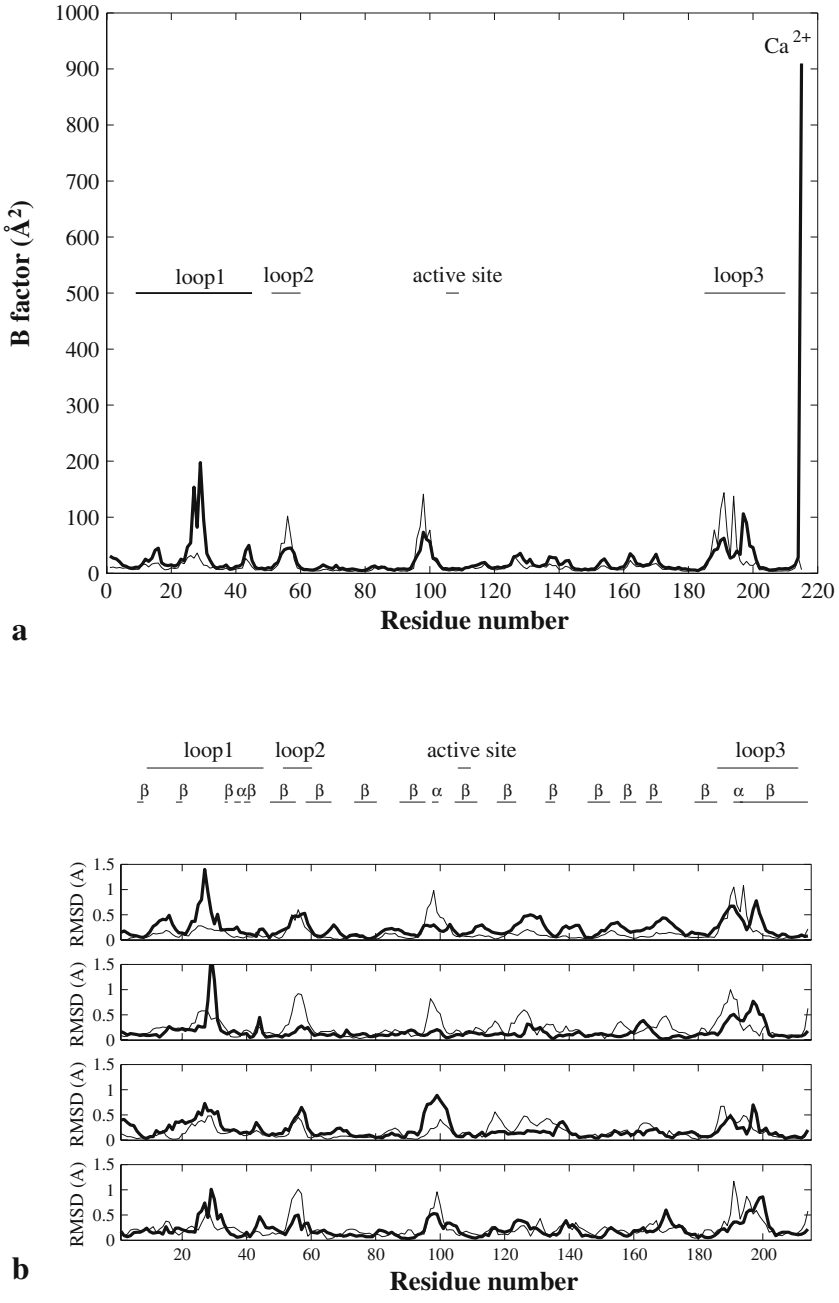

Fig. 3 Representation of the fluctuation of the fold. **a** By means of B-factors. Representation of the B-factors of side-chain residues derived from the MD simulations of β-glucanase. The results are from the averaged structures of the last 2,000 ps of each simulation. *Thin line*: low-temperature simulation. *Thick line*: high-temperature simulation. **b** By means of the first four Essential Modes. RMSD (for backbone atoms) corresponding to a trajectory built along the first four Eigenvectors calculated from the low (*thin line*) and high (*thick line*) temperature simulations (interval 2,000–4,000 ps). RMSD values referred to X-ray structure

between residues F30 and R35 interacts with region N57-C61 and extends its β-strand with loop 2. This serves to identify a large motion for loop 1, which moves up from the top of the active site together with loop 2, and this in turn pushes loop 3.

Essential dynamics and entropy

The analysis of ED shows that the first six modes retain almost 50% of the total motion of both simulations at 300 and 325 K. The percentage of simulation explained by each essential mode, the accumulated percentage, and the partial and total entropy for both simulations at 300 and 325 K are shown in Table 3. As expected, the total entropy for the simulation at 325 K is higher than for the simulation at 300 K, due to the increase in the atomic fluctuation when the temperature rises.

The projection of the dynamics on each particular mode was obtained by short-step motions in the mode direction (see "Materials and methods"). The projection results in a simulated dynamic motion, which is analyzed by atomic fluctuations. Figure 3b shows the atomic deviations from the crystallographic structure of 1-3,1-4 β-glucanase along the first four modes obtained from the simulation at 300 and 325 K. It should be noted that the motions of the first essential modes indicate the regions of glucanase involved with its activity. The motion around loops 1, 2, and 3 and the active site is represented in modes 1, 2, 3, and 4, for both simulations. However, the distribution and the

Table 2 Hydrogen bond network

				X-ray structure	300 K simulation	325 K simulation
Backbone hydrogen bonds						
10	PHE	207	ASN	–	–	73.75
17	LEU	14	ASN	*	–	–
18	TRP	14	ASN	*	80.15	75.45
19	GLN	65	ARG	*	97	69.2
21	ALA	63	GLU	*	80.55	83.65
23	GLY	34	TRP	*	–	–
24	TYR	34	TRP		76.55	69.0
30	PHE	27	GLY	*	93.3	–
31	ASN	185	ASN	*	80.95	–
32	CYS1	30	PHE	*	–	–
33	THR	59	PHE	*	97.45	92.9
34	TRP	24	TYR	*	70.35	59.5
35	ARG	61	CYS2	*	90.55	75.4
39	VAL	36	ALA	*	75.8	77.0
40	SER	48	ARG	*	79.7	86.9
42	THR	46	GLU	*	88.9	74.1
45	GLY	42	THR	*	50.75	56.6
105	GLU	123	TYR	*	88.6	86.2
107	ASP	121	ASN	*	95.15	82.5
108	ILE	91	PHE	*	98.15	89.4
109	GLUH	119	GLN	*	99.35	92.8
206	TYR	47	MET	*	90.55	76.1
207	ASN	78	ASN	*	66.8	77.5
209	VAL	8	GLU	*	98.6	94.2
Backbone to side-chain hydrogen bonds						
10	PHE	8	GLU	*	52.95	–
17	LEU	14	ASN	–	65.05	–
20	LYSH	13	TYR	*	–	70.0
27	GLY	25	SER	*	–	–
29	MET	28	ASN	*	94.4	–
30	PHE	28	ASN	–	–	50.0
36	ALA	22	ASP	*	74.8	–
106	ILE	93	THR	*	–	60.6
Side-chain to backbone hydrogen bonds						
20	LYSH	36	ALA	*	–	–
20	LYSH	39	VAL	*	–	–
38	ASN	50	SER	*	92.5	51.6
40	SER	40	SER	*	–	–
206	TYR	90	SER	*	72.4	–
Side-chain to side-chain hydrogen bonds						
13	TYR	64	ASN		97.4	–
18	TRP	8	GLU	*	–	–
33	THR	60	ASP		73.35	54.8
34	TRP	26	ASN	*	–	–
35	ARG	60	ASP	*	58.2	–
38	ASN	52	THR	*	58.8	–
42	THR	46	GLU	*	98.4	–
206	TYR	89	SER	–	–	86.6
207	ASN	78	ASN	*	–	–

Average occurrence of native intramolecular hydrogen bonds (i.e. hydrogen bonds found in the crystallographic structure) during the two MD simulations. Only those hydrogen bonds appearing in at least 40% of the conformations analyzed were taken into account. The values were taken with a cut-off distance of 2.5 Å and cut-off angle of 135° between donor and acceptor. The residues included were 9–45, 105–109, and 206–209 along the 2,000–4,000 ps fragment of the simulations. Hydrogen bonds present in the crystallographic structure are indicated with asterisks

Table 3 Essential dynamics

Eigenvector	MD simulation at 300 K			MD simulation at 325 K		
	Explained (%)	Accumulated (%)	Entropy	Explained (%)	Accumulated (%)	Entropy
1	24.69	24.69	3.38	13.62	13.62	3.29
2	9.15	33.83	6.48	11.49	25.11	6.53
3	4.68	38.51	9.37	6.93	32.04	9.63
4	4.52	43.04	12.25	4.55	36.59	12.59
5	3.97	47.01	15.09	3.44	40.03	15.48
2,565	0.00	100.00	1,142.94	0.00	100.00	1,265.83

Essential dynamics analysis of the two MD-simulations (backbone atoms). Eigenvectors are listed in order of decreasing Eigenvalues. Eigenvalues are expressed relative to the total mean-square atomic positional fluctuation (trace of the eigenvalue matrix). Values were calculated for the low and warm temperature simulations (interval 2,000–4,000 ps)

strength of the signal, seen in the atomic deviation of the projected simulation, show remarkable differences.

For the first essential mode of the simulation at 300 K, residues P54–Y56 (located at the end of loop 2), residues P97–D99 (3_{10} helix located opposite loop 1), and residues E191 and G194 (end of loop 3) show the largest motion. The lower motion of residues of W192 and L193 than of E191 and G194 should be noted. The second mode shows the motion around residues S25–N28 (end of loop 1, opposite P97–D99), loop 2, the 3_{10} helix, G126, and E191. The disappearance of the motion previously observed for residue G194 should be stressed. The third and fourth modes for the simulation at low temperature show trends that are similar to each other and similar to those mentioned above.

The first and second modes of the simulation at warm temperature show large motions on loop 1 and 3. Minor, but remarkable, motions are also observed for residues N14-G16 (loop 1), G126-E131, D139-S143, N154-I156, and A168-T170. All these residues are located at the outer sides of the protein, far from the catalytic cleft. The third mode of the simulation at 325 K is similar to the fourth one, but a characteristic motion is observed for residues T98-G100, located at one of the extremes of the catalytic cleft. This motion seems to be transferred from the first and second motion of the simulation at 300 K.

However, the residue G198 (loop 3) shows practically no motion at 300 K. However, at 325 K, it shows a clear motion in all the essential modes. This residue is located in an intermediate region facing residues P54–K58 in loop 2, which also shows motion in the first essential mode at 325 K. Hence, the release of calcium ion seems to affect the motion of loop 2 and, in consequence, the motion of the intermediate region of loop 3.

Fig. 4 Structural alignment of glucanases. Alignment obtained with STAMP of the sequences of Endo-glucanases from *Bacillus macerans* (1MAC), *Bacillus licheniformis* (1GBG), *Fibrobacter succinogenes* (1MVE, after reverting the natural cyclic permutation), and *Pseudoalteromonas carrageenovora* (1DYP). Regions of calcium binding are indicated in *gray* background, and the residue involved in the coordination in *black*

Sequence comparison among glucanases around the metal binding

To relate the sequence of *endo*-1,3-1,4-β-glucanase with the flexibility of particular regions and binding of Ca^{+2}, this has been compared with the structures of homologous proteins. The sequence of *endo*-1,3-1,4-β-glucanase from *B. licheniformis* was used to find homologue sequences in the PDB with the PSI-BLAST program. We found 11 PDB codes showing *e*-values under 10^{-30}, with 1GBG (which is the PDB code for this glucanase) among them. Four of them were obtained by a cyclic permutation of the glucanase from *Bacillus macerans* and one was a natural cyclic permutation from *Fibrobacter succinogenes*, which meant the permutation had to be reversed for correct comparison of its sequences. We used STAMP to obtain the structural multiple alignment of the nonredundant glucanases (Fig. 4): from *B. macerans* (PDB codes 1AJO, 1AXK, 1BYH, 1GLH, 1MAC, 2AYH), *B. licheniformis* (code 1GBG in the PDB), *F. succinogenes* (code 1MVE), and *Pseudoalteromonas carrageenovora* (code 1DYP, that binds Cd^{2+} instead of Ca^{2+}). The alignment shows that some of the residues involved in calcium binding and the chemical properties of its environment are conserved. The region where the first β-strand is broken by a proline turn (region I), which is only conserved for glucanases from *B. licheniformis* and *B. macerans*, shows a set of negatively charged residues that help to bind Ca^{2+}. In addition, the region around Gly45 (region II), involved in binding Ca^{2+} by means of its main-chain carbonyl, shows the conservation of the Gly residue, but the order and number of surrounding negatively charged residues is different. It is in fact the most negative environment found for the structures of 1GBG and 1MVE. Finally, the best conserved region (region III) of the sequence is found around Asn 207, formed by Asn or Asp surrounded by hydrophobic residues, mainly aromatic ones such as Tyr or Trp. This region binds the metal and at the same time preserves the hydrophobic core and contacts between β-strands.

Regions II and III are most affected by the temperature, as the values of *B*-factor and the first essential modes show, whereas region I remains unperturbed. This effect is seen in the increase of the deviation caused by the essential modes 1, 2, 3, and 4 of the simulation at higher temperature. For all essential modes, the deviation increases in regions II and III, simultaneously. In region III, the motion shifts to the right showing a larger deviation closer to region III, while at lower temperature the pick of motion was sharpened at the α-helix secondary structure.

Thermo-inactivation studies

To verify the calcium contribution to thermal stability experimentally, T_m of wild-type β-glucanase and a N207D mutant was determined experimentally. The effect of the addition of an extra electrostatic interaction between calcium and aspartic has a clear effect on the increase of T_m. Wild type T_m is 71.4°C and N207D has a T_m of 75.3°C. However sometimes, especially when we are talking about enzymes, the improvement of the thermostability of a protein could have a drastic effect on enzyme activity, especially if the mutated position plays an important role in the enzymatic mechanism. In our case, we suspect that calcium is lending the mobility that the main loop requires to carry out enzymatic catalysis. This means that activity and stability could be correlated. In the wild-type glucanase, calcium exhibits octahedral coordination to the backbone carbonyl oxygens of Pro9, Gly45, and Asn207, an amide oxygen of Asn207. Mutation N207D pretends to retain more strongly this calcium with an extra charge. Mutation N207A pretends to remove one of these original interactions, the lateral chain amide oxygen of Asn207 weakening the calcium coordinated bond. The results of inactivation at experiments at 65°C (Fig. 5) were clear: (1) N207A, destabilization of calcium has a dramatic effect on protein activity and stability; (2) N207D, this mutant displayed better thermotolerance than the wild-type protein; stabilization of calcium could increase the half-life of the protein, but also reduce its activity; (3) these data (initial velocity points) were fitted using a double exponential decay function because simple exponential decay does not follow the behavior of the points. Both the native and mutated enzyme N207D showed biphasic inactivation kinetics. These results are consistent with previous studies, which found that melting of H(A12-M) delta Y13 and H (A16-M), hybrid of the *Bacillus amyloliquefaciens* and *B. macerans* of the (1-3,1-4)-beta-glucanases in the presence of calcium ions is characterized by two subtransitions [6]. In a previous study, we found an inverse linear correlation between the relative change in pseudodipole moments and transition-temperature increases [30]. The mutation N207D produced a reduction in the pseudodipole moment which, according to the theoretical analysis, leads to protein thermostabilization. This approach could provide us another possible explanation of the

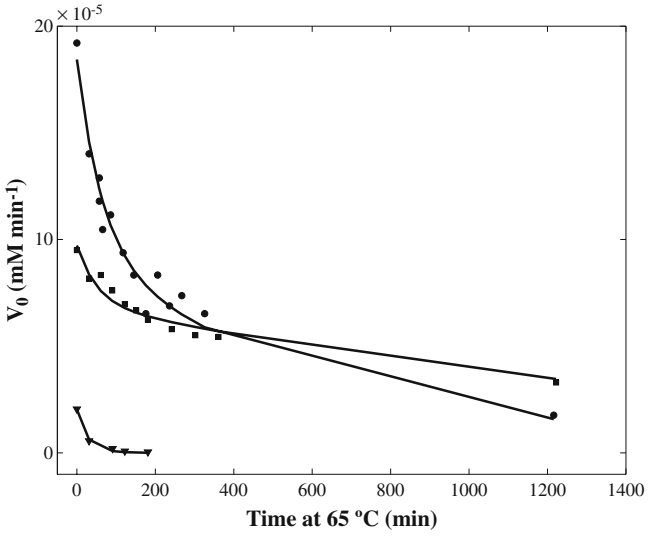

Fig. 5 Thermo-inactivation study. Experimental curves for wild-type β-glucanase (*circles*), N207D mutant (*square*), and N207A (*triangle*) enzymes incubated at 65°C

present results: N207D mutation generated an electronic compactation of the glucanase, increasing the thermostability of the protein, but at the same time this mutation may reduce protein loops fluctuations which are necessary for its enzymatic activity.

Average structure

Figure 6 shows the average structures calculated from 2,000 to 4,000 ps for both simulations. In general, the shape of the protein is maintained along both simulations. In particular, the catalytic cleft is fully conserved and only some variations can be observed at the extremes of the loops closing it. In general, the regions that modify their position due to the temperature rising are located at the outer convex site of the protein. Residues P9, G45, and N207, which at low temperature are bound to calcium ion, show different behavior on temperature increase. N207 practically does not change its position, whereas P9 and G45 do shift a little. This is interesting, as the loss of calcium ion should produce greater variation in the positions of these three residues. Finally, the most dramatic changes in the position of residues on the temperature rising can be seen at the extremes of loops 1 (S25-N31), 2 (P54-D60), and 3 (G186-P201). As expected, the increase of temperature from 300 to 325 K did not cause any significant change on the disulfide bridge.

Fig. 6 Averaged structures. Averaged structures for β-glucanase along the last 2 ns of simulations at 300 K (*blue*) and 325 K (*red*). Loops 1, 2, and 3 are shown at the *top* of the figure. Calcium ions are shown at the *bottom* of the figure. The catalytic cleft is located in the *middle*

Discussion

MD simulations are a useful tool for studying deactivation processes in enzymes. In this research, MD was applied to the description of phenomena occurring in *B. Licheniformis* β-glucanase. In addition, ED, a powerful tool for describing molecular motions, was used.

The mean structure of β-glucanase for the simulation at 300 K (Fig. 6) is very similar to the initial crystallographic X-ray structure, as deduced from the low RMSD values (around 1.25 Å), the small increase in the radius of gyration (results not shown), and the lack of clear changes in the solvation behavior of the protein throughout the time of simulation. Finally, it should be pointed that, in both structures, the Ca^{2+} ion is bonded to residues Pro9, Gly45, and Asn207, connecting loops 1 and 3.

The binding-site cleft of the protein is defined by two structural elements of the three-dimensional protein fold (Figs. 1 and 6): loop 1, which partially covers the distant subsites of substrate at the nonreducing end from the site of hydrolysis, and a large β-sheet of seven antiparallel strands at the concave face of the molecule that shape the entire cleft [1]. Hence, it is expected that the most important motions of the protein (or the lack of them) could be related to these two structural elements. It is clear from ED analysis that, at low temperatures, protein motions are mainly located around residues P54–Y56 (located at the extreme of loop 2), P97–D99 (3_{10} helix located opposite loop 1), and residues E191 and G194 (extreme of loop 3). This was also indicated by the calculated values for *B*-factors (Fig. 3a). These three regions coincide with residues located at the entrance of the active cleft. These motions could be related to the catalytic activity of the enzyme at low temperatures. Hence, the positions of residues at loop 2 would act as a trigger that pushes loop 3, which, in turn, pushes the substrate to the active sites. The motion of residues in the 3_{10} helix could be related to the closing of the catalytic cleft. On the contrary, residues directly relating to catalytic activity, such as G105, D107, and G109, or important in keeping the structural integrity of the binding cleft, such as Y94 [1], show no characteristic motion along any of the first essential modes. Finally, the lack of a clear motion in loop 1 could also relate to role of these residues in enzyme activity and stability. Hence, alanine-scanning mutagenesis studies on residues D22 to R35 have already proved this role [28]. This lack of motion could be due to the presence of the Ca^{2+} ion, which is bonded to residues P9 and G45, in addition to the disulfide bridge between residues C32 and C61 (loop 2).

It is known that the N-terminal sequence and the Ca^{2+}-binding site are essential for thermal stability in β-glucanases [6–8]. In our case, the effect of increasing temperature from 300 to 325 K does not unfold the structure, according to the results of MD simulations. Hence, RMSD, radius of gyration, and solvation parameters show that at warm temperature the structure is preserved. However, some parts of the protein experience the effects of temperature rising, as observed in the average structure for the simulation at 325 K. Special attention must

be paid to the calcium ion. Its average position shows that this is relatively far from the residues at which it was initially bound at 300 K. The high motion of calcium ion is confirmed by the corresponding *B*-factors. The effect of the release of calcium ion on the activity of the enzyme is clear, as demonstrated by the thermoinactivation studies. However, the average structure at 325 K does not show large changes in the region around P9, G45, and N207. Only P9 and G45 are slightly shifted from their average positions at 300 K. The effect of the release of calcium ion should then be found in the changes of global motion of loops 1 and 3, rather than in changes of average positions for some selected residues.

The main loop of β-glucanase shapes the carbohydrate-binding cleft and has a big influence on protein thermotolerance and activity. To analyze the role of loop residues of *B. licheniformis,* an alanine-scanning mutagenesis approach was adopted [28]. The resulting mutants were analyzed by equilibrium urea denaturation, thermotolerance at 65°C, and kinetics. Mutants F30A and W34A, involved in hydrophobic packing of the main loop, show a pronounced reduction in catalytic efficiency, which demonstrates the close relation between activity and main-loop packing [28]. The results obtained in this study point to the maintenance of the structure of the main loop upon temperature rising.

In general, ED has shown that the motion at 325 K is clearly different from that at 300 K. Hence, ED for the simulation at 325 K shows a clear shift in motions from residues in 3_{10} helix to those in loop 1. Some motions are practically maintained, such as those relating to loop 2, or slightly modified, like those relating to loop 3.

The features of the conformation remained the same, except for the calcium binding region after increasing the temperature from 300 to 325 K. However, dynamic properties were modified upon inactivation of the enzyme. Glucanase activity depends on a specific distance restriction and on a subtle acid-base equilibrium favored by the microenvironmental p*K*a. Any alteration in the distances between amino acids of this acidic environment could modified this local p*K*a and it could modify the efficiency of the enzyme catalytic activity. MD shows that the active site and loop 1 changed as a consequence of two steps: (1) the disturbance produced on the active site around the Glu105 and Glu109, and (2) loop 1 at the top of the active sites moves up, increasing the stability of the β-sheet by extending the β-strand of loop 1 with that of loop 2. The motion shown at warm temperature implies that the loop is moved upwards and stabilized by extending the β-strand. Assuming the hypothesis that the motion of loop 1 pushes the substrate towards the active site, this mechanism becomes impeded at warm temperature. These results may explain the inactivation of glucanase. Because loop 1 is involved in the changes shown and the main difference in conformation from simulation at 300 K is the loss of calcium binding, we propose the following explanation for the inactivation of glucanase by temperature: (1) in the first step the increase of temperature leads to a larger number of water molecules impacting with the calcium ion to release it from its binding with the protein; (2) the liberation of calcium lets loop 1 free at the extremity and allows for the motion shown in essential modes 1 and 2 at 325 K; (3) this motion implies the disturbance at the active site and the deformation of loop 1 that finally yields the inactivation of glucanase without unfolding.

Thermal inactivation behavior gave us a sound argument for the credibility of the results of the MD. We propose the following hypothesis that could explain the experimental results: the first phase in thermal denaturation could be produced when calcium interactions are disrupted and the main loop becomes free to rearrange. This phase yields a partially active intermediary during the first phase of inactivation and then the intermediary is slowly converted into a totally inactive enzyme in the second phase.

Acknowledgements RG received a grant from the Spanish MEC (BQU2003-00191). BO received grants from the Fundación Ramón Areces and from the Spanish MEC (BIO2002-03609 and BIO2005-00533). EQ received grants from Ministerio de Ciencia y Tecnologia (BIO2001-264) and from the Centre de Referència de R+D de Biotecnología de la Generalitat de Catalunya.

References

1. Planas A (2000) Biochim Biophys Acta 1543:361–382
2. Juncosa M, Pons J, Dot T, Querol E, Planas A (1994) J Biol Chem 269:14530–14535
3. Malet C, Vallés J, Bou J, Planas A (1996) J Biotechnol 48:209–219
4. Henrissat B, Callebaut I, Fabrega S, Lehn P, Mornon J, Davies G (1995) Proc Natl Acad Sci USA 92:7090–7094
5. Planas A, Juncosa M, Lloberas J, Querol E (1992) FEBS Lett 308:141–145
6. Welfle K, Misselwitz R, Welfle H, Politz O, Borriss R (1994) J Biomol Struct Dyn 11:1417–1424
7. Welfle K, Misselwitz R, Welfle H, Politz O, Borriss R (1995) Eur J Biochem 229:726–735
8. Welfle K, Misselwitz R, Politz O, Borriss R, Welfle H (1996) Protein Sci 5:2255–2265
9. Keitel T, Meldgaard M, Heinemann U (1994) Eur J Biochem 222:203–214
10. Lloberas J, Querol E, Bernués J (1988) Appl Microbiol Biotechnol 29:32–38
11. Gargallo R, Hünenberger P, Aviles F, Oliva B (2003) Protein Sci 10:2161–2172
12. Amadei A, Linssen A, Berendsen H (1993) Proteins Struct Funct Genet 17:412–425
13. Yang C, Gouri S, Kuczera K (2001) J Biomol Struct Dyn 19:247–271
14. van Gunsteren W, Billeter S, Eising A, Hünenberger P, Früger P, Mark A, Scott W, Tironi I (1996) Biomolecular simulation: the GROMOS96 manual and user guide. Verlag der Fachvereine, Zürich
15. Berendsen H, Grigera J, Straatsma T (1987) J Phys Chem 91:6269–6271
16. Rickaert J, Ciccotti G, Berendsen H (1977) J Comput Chem 23:327–341
17. Tironi I, Sperb R, Smith P, van Gunsteren W (1995) J Chem Phys 102:5451–5459

18. Hünenberger, P, van Gunsteren W (1998) J Chem Phys 108:6117–6134
19. Gargallo R, Oliva B, Querol E, Avilés F (2000) Protein Eng 13:21–26
20. Richmond T (1984) J Mol Biol 176:63–89
21. Nicholls A, Honing B (1991) J Comput Chem 12:435–440
22. Bashford D (1997) An object-oriented programming suite for electrostatic effects in biological molecules. In: Ishikawa Y, Reynders J, Tholburn M (eds) Scientific computing in object-oriented parallel environments. Springer, Berlin Heidelberg New York, pp 233–240
23. Schlitter J (1993) Chem Phys Lett 215:617–621
24. Schäfer H, Mark A, van Gunsteren W (2000) J Chem Phys 113:7809–7817
25. Schäfer H, Daura X, Mark AE, van Gunsteren W (2001) Proteins 43:45–56
26. Schäfer H, Smith LJ, Mark A, van Gunsteren W (2002) Proteins 46:215–224
27. Sherer E, Harris S, Soliva R, Orozco M, Laughton C (1999) J Am Chem Soc 121:5981–5991
28. Pons J, Planas A, Juncosa M, Querol E (1997) Methods Mol Biol 67:209–218
29. Malet C, Viladot J, Ochoa A, Gállego B, Brosa C, Planas A (1995) Carbohydr Res 274:285–301
30. Mozo-Villarias A, Cedano J, Querol E (2003) Protein Eng 16:279–286